

# RSC Advances



This is an *Accepted Manuscript*, which has been through the Royal Society of Chemistry peer review process and has been accepted for publication.

*Accepted Manuscripts* are published online shortly after acceptance, before technical editing, formatting and proof reading. Using this free service, authors can make their results available to the community, in citable form, before we publish the edited article. This *Accepted Manuscript* will be replaced by the edited, formatted and paginated article as soon as this is available.

You can find more information about *Accepted Manuscripts* in the [Information for Authors](#).

Please note that technical editing may introduce minor changes to the text and/or graphics, which may alter content. The journal's standard [Terms & Conditions](#) and the [Ethical guidelines](#) still apply. In no event shall the Royal Society of Chemistry be held responsible for any errors or omissions in this *Accepted Manuscript* or any consequences arising from the use of any information it contains.

## Effect of Molecular Chain Length on the Properties of Amine-Functionalized

### Graphene Oxide Nanosheets/Epoxy Resins Nanocomposites

Fengdan Liu<sup>1,3</sup>, Ling Wu<sup>2</sup>, Yanjie Song<sup>1</sup>, Wenguang Xia<sup>2</sup>, Kunkun Guo<sup>1,4\*</sup>

<sup>1</sup>College of Materials Science and Engineering, Hunan University, Changsha, 410082, China

<sup>2</sup>Patent Technology Development Company of China, Beijing, 100088, China

<sup>3</sup>FAW-Volkswagen Automobile Co., Ltd., Changchun, 130000, China

<sup>4</sup>State Key Laboratory of Molecular Engineering of Polymers, Fudan University, Shanghai, 200433, China

#### Abstract

Amine-functionalized graphene oxide nanosheets (D400-GOs and D2000-GOs) were prepared by linear poly(oxyalkylene)amines with two different molecular weights 400 and 2000 (D400 and D2000) attached onto the surface of graphene oxides via the reactions of amines with alkylcarboxyle groups. By mixing the amine-functionalized graphene oxide nanosheets, the epoxy resins (EPs) and curing agent, the amine-functionalized graphene oxide nanosheets/EPs nanocomposites were subsequently fabricated. In these nanocomposites, the amine-functionalized graphene oxide nanosheets could covalently integrate into EPs matrices via the reactions between amine groups of the chemical converted graphene oxide nanosheets and epoxy groups of EPs, thereby causing that these graphene oxide nanosheets become part of the heavily cross-linked network. The mechanical and thermal properties of these nanocomposites are investigated in detail. The effect of molecular chain length of grafted polymers on these properties of the chemical converted graphene oxide nanosheets/EPs nanocomposites are thoroughly discussed. This study provides a new route to design and develop chemical converted graphene oxide nanosheets/polymer nanocomposite materials by varying the chain length of polymers grafted onto the surface of graphene

---

\* Corresponding author Email: kunkunguo@hnu.edu.cn

oxide nanosheets and then tuning the interphases between graphene oxide nanosheets and polymer matrices.

**Keywords:** Amine-functionalized graphene oxide nanosheets; Epoxy resins; Poly(oxyalkylene)amines; Molecular chain length; Mechanical and thermal properties

## 1. Introduction

Nanocomposites, as advanced materials, have attracted wide interests in both academic and commercial communities recently [1-4]. Polymer-based nanocomposites that possess the ease of processing along with the dramatically improved and multifunctional properties open the way to completely new applications of polymers [3-7]. Mechanical enhancements of polymer-based nanocomposites are expected when nanoparticles can be fully exfoliated in polymer matrices. The most challenges of polymer-based nanocomposites are that the inorganic hydrophilic nanoparticles are thermodynamically inhibited to be homogeneously dispersed in the organic hydrophobic polymer matrices, as well as the external load can not be effectively transferred by interfacial interactions between nanoparticles and polymer matrices.

Graphene [8-9], a single-atom-thick form of carbon layer organized in a honeycomb structure, shows unique physical, chemical, and mechanical properties, providing various applications of graphene and graphene derivatives, such as hydrogen storages [10], sensors [11], supercapacitors and batteries [12], and polymer nanocomposites [13-14]. Since the discovery of graphene in 2004 [8-9], a series of studies have continuously devoted to fabricate graphene, which are generally categorized into two main methods. One is to directly produce graphene either by a top-down approach (e.g., mechanical cleavage of graphite) or by a bottom-up approach (e.g. organic synthesis, epitaxial growth, and chemical vapor deposition). The other method is to first prepare graphene oxide nanosheets (GOs) by the oxidation of graphite with strong oxidants and then convert GOs to graphene by reduction. The oxygen functional groups on the

graphene oxides surface can provide versatile sites for chemical functionalization, thereby producing chemical converted graphene nanosheets [15-18], such as the amine-functionalized graphene nanosheets [19] and polystyrene-functionalized graphene nanosheets [16]. These chemical converted graphene nanosheets impart the improved compatibility and reinforcing efficiency of graphene in polymeric matrices. For example, the conducting graphene polymer nanocomposites have been prepared by solution mixing of exfoliated functionalized graphite oxide sheets with polystyrene, acrylonitrile-butadiene-styrene, and styrene-butadiene copolymers [15-18].

Epoxy resins (EPs) [20-21] is one of the most widely used polymers in structural complexes, coating, adhesives, hardware components, semiconductor encapsulation due to its high performance properties such as tensile strength, high stiffness, etc. However, the brittleness and weak flame resistance of epoxy resins limit its industrial applications. In our previous studies [22-23], a sufficient strategy has been proposed to synthesize the chemical converted graphene oxide nanosheets to reinforce epoxy resins. m-Xylylenddiamine (m-XDA) that acts as the traditional curing agent for EPs, is chosen to be covalently bonded to the GOs surfaces via amine reactions with carboxyl groups on the surface of the GOs. The terminal amine groups on the surface of chemical converted graphene oxide nanosheets can directly react with the epoxy groups, thereby giving that the chemical converted graphene oxide nanosheets work in such a way as the curing agent for EPs. Therefore, the amine-functionalized graphene oxide nanosheets would be part of the heavily cross-linked composite structure. In the present study, a similar strategy has been employed that linear poly(oxyalkylene)amines with two

different molecular weights are covalently attached to the surface of graphene oxides. As expected, the molecular chain length of the grafted polymers might influence the properties of amine-functionalized graphene oxide nanosheets/EPs nanocomposites.

## 2. Experimental details

### 2.1. Materials

Graphite flakes (325 mesh and about 44  $\mu\text{m}$ ) were obtained from Qingdao Jinrilai Graphite Co. Ltd. Concentrated Sulfuric acid ( $\text{H}_2\text{SO}_4$ , 98%) was purchased from Tianjin Jinfeng Chemical Reagent Co. Ltd. Potassium permanganate ( $\text{KMnO}_4$ ) was provided by Changsha Xiangke Chemical Reagent Co. Ltd. Potassium persulfate ( $\text{K}_2\text{S}_2\text{O}_8$ ), anhydrous calcium chloride ( $\text{CaCl}_2$ ) and anhydride phosphorus pentoxide ( $\text{P}_2\text{O}_5$ ) were obtained from Tianjin Kermel Chemical Reagent Co. Ltd. Hydrogen peroxide ( $\text{H}_2\text{O}_2$ , 30%) was provided from Hunan Huihong Chemical Reagent Co. Ltd. Thionyl chloride ( $\text{SOCl}_2$ ), N, N-dimethylformamide (DMF), and two poly(propylene glycol) bis(2-aminopropyl ether) with the average molecular weights of  $\sim 400$  (D400) and  $\sim 2000$  (D2000) were purchased from Tianjin Hengxing Chemical Reagent Co. Ltd. Diglycidyl ether of bisphenol A epoxy resins (EPs) (an epoxy equivalent per weight of 197) and m-Xylylenediamine (m-XDA) as the curing agent were obtained from Chemical Technology Research Institute of Changsha.

### 2.2. Synthesis of chemical converted graphene oxide nanosheets

Similar to our previous strategy [22], the synthesis illustration of chemical converted graphene oxide nanosheets is given in Scheme 1, and the detailed procedure are given as follows. Firstly, graphene oxides were prepared referring to the modified Hummers'

method [24]. Then, 100 mg GOs obtained was refluxed in 20 ml  $\text{SOCl}_2$  in the presence of 0.5 ml DMF at  $70^\circ\text{C}$  for 24 h, using an anhydrous calcium chloride guard tube. At the end of the reaction, the excess of  $\text{SOCl}_2$  was removed by distillation. Then, 20 ml anhydrous DMF was added into the remaining solid. After sonication for 10 minute, the mixture was slowly dropped into 20 ml D400/D2000 in an ice bath. Kept sonicating for another 10 minutes, a homogeneous solution was obtained and then heated to  $120^\circ\text{C}$  for 12 h. The final products were washed with a large amount of hot ethanol. The resulting products were the amine-functionalized graphene oxide denoted as D400-GOs/D2000-GOs, respectively.

### **2.3. Fabrication of D400-GOs/EPs (D2000-GOs/EPs) nanocomposites**

D400-GOs/D2000-GOs with the required amount, which was obtained by above procedure, was dispersed in acetone to form a suspension with a concentration of 0.125 mg/ml. Subsequently, the EPs was added to this suspension and treated by sonication for 2 h, and then was further rigorously stirred for another 2 hours. The resulted mixture was put into a vacuum at  $60^\circ\text{C}$  in order to eliminate the extra acetone. After the mixture was naturally cooled to room temperature, the curing agent (m-XDA) was added, where the mole ratio for epoxy groups to hydrogen atoms of amino groups was 1:1. The resultant suspension was degassed in the vacuum oven to clear the bubbles and residual acetone. Then, the suspension was transferred to an open mold and cured at  $60^\circ\text{C}$  for 2 h, then  $150^\circ\text{C}$  for 3 h. After curing, the samples were cooled naturally to room temperature, and the fully cross-linked D400-GOs/EPs or D2000-GOs/EPs nanocomposites were finally obtained. The D400-GOs/EPs or D2000-GOs/EPs

nanocomposites were prepared to contain the D400-GOs or D2000-GOs with weight fractions of 0 wt%, 0.1 wt% and 0.2 wt%, respectively. These nanocomposites were correspondingly abbreviated as EPs, 0.1 % D400-GOs/EPs and 0.2 % D400-GOs/EPs, 0.1 % D2000-GOs/EPs and 0.2 % D2000-GOs/EPs.

#### 2.4. Characterization

Fourier transform infrared (FTIR) spectrum was recorded between 4000  $\text{cm}^{-1}$  and 500  $\text{cm}^{-1}$  on a Nicolet 6700 infrared spectrometer. Raman spectrum was carried out by a Renishaw inVia-Reflex with a 785 nm Ar laser. X-ray diffraction (XRD) spectrum was characterized by Siemens D5000 with Cu  $\kappa\alpha$  radiation. X-ray Photoelectron (XPS) spectrum was conducted using ESCALAB 220i-XL spectrometer. To measure the tensile strength and modulus, five samples were prepared according to the standard of ASTM D638, and were tested using an Instron 3382 instrument at room temperature with a speed of 2.5 mm/min. The morphologies of both the tensile and freeze fractured surfaces were investigated by High-Resolution Scanning Electron Microscopy (S4800) with an accelerating voltage of 30 kV. Prior to the observations, the fracture surfaces were sputter-coated with a thin layer of gold. Thermogravimetric analyses (TGA) were performed with a TA TQAQ50 thermal analyzer from 25  $^{\circ}\text{C}$  to 800  $^{\circ}\text{C}$  at a heating rate of 10  $^{\circ}\text{C}/\text{min}$  in nitrogen ( $\text{N}_2$ ). The glass transition temperatures ( $T_g$ ) of the nanocomposites were obtained by PE DSC-Q10 differential scanning calorimetry (DSC). The  $T_g$  was determined by the midpoint method provided by TA universal analysis software. Transmission electron microscope (TEM) observations were conducted using a JEM-3010 microscope (JEOL Limited, Tokyo, Japan) with 200 kV.

### 3. Results and Discussions

#### 3.1. Morphologies of amine-functionalized graphene oxide nanosheets

Transmission electron microscope of the GOs, D400-GOs, and D2000-GOs are used to characterize the surface morphologies and the results are shown in Figure 1. Figure 1(a) shows that GOs attain a smooth carpet-like structure. Compared to GOs, much rougher and encapsulating structures are observed in Figure 1(b) and 1(c), suggesting the successful grafting of poly(oxyalkylene)amine chains to GOs surfaces. The long molecular chains of poly(oxyalkylene)amine are observed to easily form encapsulating and globular morphology on the GOs surface. As shown in these TEM morphologies, GOs, D400-GOs and D2000-GOs all show two-dimensional nanostructure. Likewise, GOs, D400-GOs and D2000-GOs possess a thickness about 3-5 nm stacked by a few graphene layers as demonstrated the AFM images (see Supporting Information).

#### 3.2 Characterization of amine-functionalized graphene oxide nanosheets

Figure 2 presents X-ray diffraction (XRD) patterns (a), Thermogravimetric (TGA) curves (b), Fourier transform infrared (FTIR) spectra (c) and Raman spectra (d) of graphite, graphite oxides (GOs), D400-GOs and D2000-GOs, respectively. As shown in Fig. 2(a), in the pattern of natural graphite, the (002) diffraction peak appears at  $2\theta=26.72^\circ$ , indicating an interlayer distance about 0.33 nm. After the oxidation from graphite to graphene oxides, the (002) peak shifts from  $26.72^\circ$  to  $10.16^\circ$  in the pattern of GOs, suggesting that the interlayer spacing undergoes such an expansion from 0.33 to 0.87 nm. This larger interlayer distance of GOs can be attributed to the wrinkling or

presence of functional groups between the interlayer structures induced by oxidation [7, 8]. After ultrasonic processing and subsequent functionalization with poly(oxyalkylene)amines (D400 and D2000), the resulting exfoliated D400-GOs and D2000-GOs do not show any sharp peaks as GOs and natural graphite do, but show very weak and broad peaks near  $24^\circ$ , close to that of graphene nanosheets [25]. These changes in the pattern of D400-GOs and D2000-GOs may attribute to the partial reduction of graphene oxides, as well as the damage of the regular crystalline structure after the oxidation of graphite and subsequent amine functionalization of graphene oxides [25].

Typical Thermogravimetric (TGA) curves of graphite, graphite oxides (GOs), D400-GOs and D2000-GOs are shown in Fig. 2(b) to describe the weight loss of materials. Slight weight loss is observed for nature graphite even when the temperature increases up to  $700^\circ\text{C}$ . For GOs, a significant weight loss can be found above  $100^\circ\text{C}$ , perhaps attributed by the decomposition of oxygen functional groups on the graphene oxides surfaces. Likewise, these oxygen functional groups contain strong hydrophilic properties, thereby giving that water molecules could be bound tightly into the stacked structures of GOs. Compared to the behavior of GOs, the poly(oxyalkylene)amine chains attached GOs sheets exhibit different weight loss curves. When the thermal temperature is less than  $300^\circ\text{C}$ , slight weight loss is observed, perhaps caused by the thermal degradation of the un-reacted oxygen functional groups. The evident weight loss occurs in the range from  $300^\circ\text{C}$  to  $450^\circ\text{C}$ , which might be caused by the degradation of linear poly(oxyalkylene)amines chains attached onto the GOs surfaces,

see Supporting Information. In addition, D2000-GOs that possess much longer attached chains [26] show higher temperature of the maximum weight loss. Therefore, we can infer that the replacement of poly(oxyalkylene)amine chains to oxygen functional groups alters the surface properties of GOs, leading to the reduction of weight loss at low temperatures. Meanwhile, the partial reduction of graphene oxides is also contributed to the decreased weight loss at high temperatures.

As shown in Fig. 2(c), in the FTIR spectrum of the natural graphite, the wide band at  $3440\text{ cm}^{-1}$  is observed due to the presence of hydroxyl groups (-OH) on the graphite surfaces. The hydroxyl groups originate from ambient atmospheric moisture bound to the graphite. Compared with the natural graphite, the adsorption bands at  $1480\text{ cm}^{-1}$  and  $1063\text{ cm}^{-1}$  (-OH),  $1130\text{ cm}^{-1}$  (-C-O-C),  $849\text{ cm}^{-1}$  (epoxy groups) appear in FTIR spectrum of GOs. The intensity of band at  $3440\text{ cm}^{-1}$  is observed to be evidently increased, suggesting that more -OH groups can be found on the GOs surfaces. In addition, the water molecules could be bound tightly into the stacked structures of GOs in the presence of these strong hydrophilic groups on the surface of GOs, which are inevitably contributed to the increased intensity of this band. After treatment with poly(oxyalkylene)amines, the intensities of these oxygen functional groups, such as epoxy ( $849\text{ cm}^{-1}$ ), -OH ( $3440\text{ cm}^{-1}$ ), -OH ( $1460\text{ cm}^{-1}$ ), are found to be decreased in both D400-GOs and D2000-GOs patterns shown in Fig. 2(c). Likewise, the new characteristic peaks at  $1630\text{ cm}^{-1}$  and  $1226\text{ cm}^{-1}$  is accompanied by the FTIR spectra of both D400-GOs and D2000-GOs patterns, corresponding to the amide carbonyl stretching mode [27] and bending vibration of N-H, respectively.

As shown in Fig. 2(d), in the Raman spectrum of the natural graphite, a prominent G peak at  $1581\text{ cm}^{-1}$  is displayed, corresponding to the first-order scattering of the  $E_{2g}$  vibration mode, as well as a weak D band adsorption at  $1331\text{ cm}^{-1}$  is observed, indicating the presence of defects inherent in the graphite and the edge effect of graphite ( $A_{1g}$  mode) [28]. Upon the oxidization from graphite to GOs, significant structural changes are observed in Fig. 2(d) that the G band is broadened and shifted to high frequency ( $1585\text{ cm}^{-1}$ ), and the D band possesses relative higher intensity. Likewise, the  $I_{D/G}$  intensity ratio is found to increase up to 1.14. These results indicate the possible distortion of bonds and the destruction of symmetry due to the reduction in size of in-plane  $sp^2$  domains caused by the extensive oxidation. Upon the treatment with poly(oxyalkylene)amines, the G band slightly shifts back to the original location of the G band in the graphite, and the D band shifts to low frequency, showing an increased  $I_{D/G}$  intensity ratio close to 1.80. The ratio of intensity from the D band to the G band ( $I_{D/G}$ ) corresponds to the amount of  $sp^3$  hybridized carbon atoms in the  $sp^2$  conjugated graphene, therefore providing direct evidence of the degree of the functionalization and structural imperfections. These results clearly indicate that linear poly(oxyalkylene)amine chains have covalently bonded onto graphene oxides surfaces.

X-ray photoelectron spectroscopic (XPS) measurements are performed for GOs, D400-GOs and D2000-GOs, and the results are presented in Figure 3. Only C1s and O1s peaks are observed in the XPS survey spectrum of GOs, but the N1s ( $399.5\text{ eV}$ ) peaks appear in the XPS spectrum of both D400-GOs and D2000-GOs. The high-resolution C1s spectra for GOs, D400-GOs and D2000-GOs are reproduced in Fig.

3 (b)-(d). As shown in Fig. 3(b), the pronounced peaks are observed at 284.8 eV, 286.2 eV, 287.8 eV and 289.0 eV, which are attributed to C-C, C-O, C=O and O-C=O bonds, respectively. These results are in well agreement with the previous result [22]. As shown in Fig. 3(c) and (d), compared with the XPS C1s spectrum of GOs (see Fig. 3(b)), the peak intensities of both C-O (286.2 eV) and C=O (287.8 eV) significantly decrease, together with the appearance of C-N peak (285.6 eV). Likewise, as shown in Fig. 3(c) and (d), the COOH peak at 289.0 eV almost disappears upon the amide formation. These results indicate the attachment of linear poly(oxyalkylene)amine chains onto graphene oxides surfaces via the reaction of terminal amines with alkylcarboxyl groups in GOs. Meanwhile, the XPS N1s spectra of D400-GOs and D2000-GOs shown in Fig. 3(e) and (f), illustrate the presence of N atoms in terms of N-H (286.5 eV in C1s and 400.8 eV in N1s), and C-N (287.6 eV in C1s and 399.6 eV in N1s).

In summary, the results obtained from TEM, XRD, Raman, FTIR, TGA and XPS, clearly demonstrate that the chemical converted graphene oxide nanosheets have been successfully synthesized by covalently bonding linear poly(oxyalkylene)amine chains onto graphene oxides surfaces via the amide formation between poly(oxyalkylene)amines and oxygen functional groups in GOs.

### **3.3 Mechanical properties of amine-functionalized graphene oxide nanosheets/EPs nanocomposites**

The tensile performances of amine-functionalized graphene oxide nanosheets/EPs nanocomposites are thoroughly studied. To assure the accuracy of the data, five specimens have been tested for every sample. Figure 4 illustrates the uniaxial tensile

testing of D400-GOs/EPs and D2000-GOs/EPs nanocomposites, respectively. It is found that the strain to break of these nanocomposites increase as a function of the loading content of the amine-functionalized graphene oxide nanosheets. Thus, we can infer that the ductility of both D400-GOs/EPs and D2000-GOs/EPs nanocomposites are evidently increased. Likewise, at 0.1 wt% loading of amine-functionalized graphene oxide nanosheets, the tensile strengths of D400-GOs/EPs and D2000-GOs/EPs nanocomposites increase up to 68.9 and 67.85 MPa, respectively. They are found to be about 23.5% and 21.60% larger than the pure epoxy resins about 55.8 MPa, respectively. However, when the loading of amine-functionalized graphene oxide nanosheets increases up to 0.2 wt%, the tensile strengths of both D400-GOs/EPs and D2000-GOs/EPs nanocomposites are found to be slightly decreased. Additionally, the fracture toughness (energy absorbed at failure evaluated by the total area under the stress vs. strain curve) of D400-GOs/EPs nanocomposite at 0.1 wt% and 0.2 wt% D400-GOs loading are about 2.5 MPa and 2.56 MPa, respectively, as well as about 262.2 % and 260.6% larger than the pure epoxy resins about 0.71 MPa, respectively. Whereas, the fracture toughness of D2000-GOs/EPs nanocomposite at 0.1 wt% (~1.19 MPa) and 0.2 wt% (~1.73 MPa) D2000-GOs loading are about 67.60 % and 143.7 % larger than the pure epoxy resins (~0.71 MPa), respectively. Therefore, the tensile performances of these nanocomposites have been improved due to the incorporation of amine-functionalized graphene oxide nanosheets into EPs matrices. At low loading content (0.1 wt%), the tensile performances of these nanocomposites are found to be better than those at high loading content (0.2 wt%). As a result, these nanocomposites

that possess the amine-functionalized graphene oxide nanosheets with short poly(oxyalkylene)amine chains, show better mechanical properties than those with much longer poly(oxyalkylene)amine chains. The changes in the mechanical properties of these nanocomposites with regard to the molecular chain length of the grafted polymer are well consistent with the previous result [29].

These remarkable changes in the tensile properties of these nanocomposites at low loadings can be due to the wrinkled and rough surfaces of the partial reduced graphene oxide nanosheets. The wrinkled and rough surfaces usually act as one favorable medium to form strong interfaces between graphene oxides and polymer matrices [30,31]. However, these changes of mechanical properties in these nanocomposites can be not completely explained by this mechanisms. At the same time, the free amino-terminated groups of the attached poly(oxyalkylene)amine chains can react with epoxy groups of EPs during the curing reaction, and then partially play a role of an effective curing agent for EPs, as shown in Scheme 2. Therefore, the amine-functionalized graphene oxide nanosheets will be integrated into EPs matrices and become part of the polymer cross-linked network rather than just rigid fillers. Then, the external load can be efficiently transferred from EPs matrices to graphene through these strong chemical bonds. The higher average molecular weight of linear poly(oxyalkylene)amine chains indicates much longer chains attached to the surface of GOs [26]. However, the other free ends of much longer attached poly(oxyalkylene)amine chains possibly react with other oxygen-containing groups in GOs, thereby forming bridges within the surface of the graphene oxide nanosheets or between graphene oxide nanosheets, see Scheme 2.

These reactions might reduce the effective grafting of poly(oxyalkylene)amine chains, leading to the difference between the mechanical properties of D400-GOs/EPs and D2000-GOs/EPs nanocomposites. In addition, short chains are found easily to form graphite intercalation compound, leading to more effective attachment of short chains (D400) onto the graphene oxides surfaces.

Young's tensile modulus is derived by the linear slope of the stress vs. strain curves. As shown in Fig. 4(a) and (d), these tensile modulus are observed to be slightly decreased, but the strains are found to be evidently increased, indicating that the chemical converted graphene oxide nanosheets are to some extent regarded as reactive plasticizers. Accompanied by the reduction of the cross-link density of the cured EPs nanocomposites, the chain flexibility in EPs matrices is subsequently improved [32].

### 3.4 Morphological analysis of the fracture surfaces

To achieve more information relevant to the interface properties between amine-functionalized graphene oxide nanosheets and EPs matrices, scanning electron microscope (SEM) is used to observe the tensile fracture surfaces of EPs, D400-GOs/EPs and D2000-GOs/EPs, and the results are presented in Figure 5 and 6. Figure 5 (a1) and (a2) show that the fracture surfaces of the pure EPs are flat and smooth without interrupted crack propagation path, requiring poor absorptions of energy during fracture. These characteristics typically correspond to the brittle failure. Compared with the pure EPs, much more ridges, ravine patterns and cracks are observed on the surfaces of both D400-GOs/EPs (see Figure 5 (b1) and (b2)) and D2000-GOs/EPs (see Figure 5 (c1) and (c2)) nanocomposites. The rougher surfaces

require much more energy to absorb during fracture, therefore leading to the improvement in the mechanical properties of these nanocomposites. In addition, no obvious graphene oxide nanosheets are observed, indicating that the chemically converted graphene oxide nanosheets have strong interfacial bonded with EPs matrices and are relative homogeneous dispersed in EPs matrices. Likewise, the freeze fracture surfaces of EPs, D400-GOs/EPs and D2000-GOs/EPs are also observed by HRSEM (see Supporting Information). Compared with EPs, the SEM images of D400-GOs/EPs and D2000-GOs/EPs show heterogeneity and the formation of defects on the freeze fracture surfaces.

As mentioned in the preceding section of mechanical properties, the tensile strength slightly reduces together with the further increasing loadings content of the amine-functionalized graphene oxide nanosheets, possible due to the presence of voids in these nanocomposites. The formations of voids primarily originate from evaporation of solvents, the volumetric shrinkage and thermal shrinkage among different substances during the curing process [23,33]. The incorporation of the amine-functionalized graphene oxide nanosheets (inorganic fillers) into polymer matrices (organic phases) would be therefore contributed to the formations of voids. At the loading content of the amine-functionalized graphene oxide nanosheets up to 0.2 wt.%, voids about 3-4  $\mu\text{m}$  in size (see Fig. 6), are easily observed in the tensile fracture surface of these nanocomposites, thereby limiting the further enhancement of the tensile strength.

### **3.5 Thermal properties of amine-functionalized graphene oxide nanosheets/EPs**

**nanocomposites**

Figure 7 shows the DSC and TGA curves of these nanocomposites, and the obtained results are summarized in Table 1. The glass transition temperature ( $T_g$ ) of the D400-GOs/EPs nanocomposites shifts to the lower temperature, but that of D2000-GOs/EPs nanocomposites increases up to the higher temperature, compared with pure EPs. As previously presented, the other free end of the long chains, D2000, would easily form bridges on the surface of graphene oxide nanosheets, thereby causing that part of D2000-GOs act as separate rigid fillers in EPs matrices, not as the cross-linked network. Whereas, D400-GOs with short chains tend to be covalently integrated into EPs matrices, and act as reactive plasticizers, thereby causing that the reduction of the cross-link density of the cured EPs, accompanied by the improvement of the flexibility of chain segments in EPs matrices, as has been discussed in section 3.2 [30]. These changes would lead to the difference of the glass transition temperature between D400-GOs/EPs and D2000-GOs/EPs nanocomposites. Additionally, the  $T_g$  of graphene oxide nanosheets grafted by *m*-Xylylenediamine (short chains)/EPs nanocomposites is also observed to shift to the lower temperature compared with pure EPs in the previous studies [22,28]. Therefore, graphene oxide nanosheets grafted by short chains are prone to decrease the glass transition temperature of these chemical converted graphene oxide nanosheets/EPs nanocomposites. At the same time, the presence of amine-functionalized graphene oxide nanosheets can influence the thermal stability of both D400-GOs/EPs and D2000-GOs/EPs nanocomposites. The temperature of 5 wt% weight loss ( $T_{5\%}$ ) and peak temperature of maximum rate of weight loss ( $T_p$ ) increase

compared with that of EPs, because the heat release is reduced in the presence of the layered structure of graphene oxide nanosheets [31]. In addition, it is found that the 0.1 wt% amine-functionalized graphene oxide nanosheets/EPs nanocomposites show much better thermal stability than that of 0.2 wt% amine-functionalized graphene oxide nanosheets/EPs nanocomposites. It is found that along with the increase of the loading content whether in D400-GOs or D2000-GOs, the chain flexibility in EPs matrices would be improved, leading to the reduction of thermal stability in these nanocomposites [31].

#### **4. Summary and conclusions**

In this study, two linear poly(oxyalkylene)amine chains with different molecular weights were successfully attached onto the graphene oxides surfaces via amine reactions with carboxyl groups at the surface of the GOs, producing two types of amine-functionalized graphene oxide nanosheets (D400-GOs and D2000-GOs). These amine-functionalized graphene oxide nanosheets were covalently incorporated into EPs matrices, forming D400-GOs/EPs and D2000-GOs/EPs nanocomposites. The mechanical results of these nanocomposites showed that these amine-functionalized graphene oxide nanosheets remarkably enhanced the tensile strength, fracture toughness, and strain of EPs at lower loading fractions (0.1 wt%). The effect of the amine-functionalized graphene oxide nanosheets on the mechanical properties of EPs are believed to be strong interface interactions between the amine-functionalized graphene oxide nanosheets and EPs. The glass transition temperature of D400-GOs/EPs nanocomposites showed a slight decrease, while that of D2000-GOs/EPs

nanocomposites presented a slight increase. The differences between two types of nanocomposites are attributed to different molecular weights of linear poly(oxyalkylene)amine chains attached onto the graphene oxides surfaces. Much longer chains, more bridges easily form on the surface of graphene oxides, then lack of free ends. Thus, D2000-GOs with more bridges possible act as separate rigid fillers in EPs matrices. Only D2000-GOs that possess other free ends, would become part of the cross-linked network structure. Whereas, D2000-GOs that acts as separate rigid fillers cannot improve the flexibility of chain segments in EPs matrices, and conversely increase  $T_g$  of these nanocomposites. Additionally, this study provides a method to develop polymer-based nanocomposites with superior performances, and to modulate interfacial interactions between GOs and EPs by constructing the chain length of grafting polymers onto the surface of GOs.

### **Acknowledgments**

We thanks Dr. Li Li and Dr. Yan Chen (Fudan University) to provide helps for AFM measurements. The financial supports of this work are provided by State Key Laboratory of Molecular Engineering of Polymers (Fudan University, no. K2015-07), and the National Natural Science Foundation of China (grant no. 21274038).

## References

1. H. Zou, S. S. Wu, J. Shen, *Chem. Rev.* 108, 3893-3957 (2008).
2. R. A. Vaia, H. D. Wagner, *Mater. Today*, 7, 32-37(2004)..
3. A. J. Crosby, J. Y. Lee, *Polym. Rev.*, 47, 217-229 (2007).
4. J. Pyun, *Polym. Rev.*, 47, 231-263 (2007).
5. Y. Y. Sun, Z. Q. Zhang, C. P. Wong, *Polymer*, 46(7), 2297-2305 (2005).
6. F. N. Ahmad, M. Jaafar, S. Palaniandy, *Compos. Sci. Technol.* 68(2), 346-353 (2008).
7. X. Q. Zhang, X. Y. Fan, Y. Chun, H. Z. Li *ACS appl. Mater. Interfaces* 4, 1543-1552 (2012).
8. K. S. Novoselov, A. K. Geim, S. V. Morozov, D. Jiang, Y. Zhang, S. V. Dubunos, *Science*, 306, 666-669 (2004).
9. S. Park, R. S. Ruoff *Nature Nanotechnol.* 4, 217-224 (2009).
10. J. S. Chen, G. C. Zhang, H. Liu, *J. Mater. Chem.* 21, 5687-5692 (2011).
11. H. J. Song, L. C. Zhang, C. L. He, Y. Lv, *J. Mater. Chem.* 21, 5972-5977 (2011).
12. K. Zhang, L. L. Zhang, J. S. Wu, *Chem. Mater.*, 22, 1392-1401 (2010).
13. H. J. Salavagione, G. Martinez. M. A. Gomez, *J. Mater. Chem.*, 19, 5027-5032 (2009).
14. T. Ramanathan, A. A. Abdala, S. Stankovich, D. A. Dikin *Nature Nanotechnol.* 3, 327-331 (2008)
15. Hummers, W.; Offeman, R. E. *J. Am. Chem. Soc.*, 80, 1339-1339(1958).
16. A. D. Lueking, L. Pan, D. L. Narayanan, C. E. B. Clifford, *J. Phys. Chem. B*, 109, 12710-12717(2005); L. L. Pan, J. H. Yu et. al., *RSC Advances*, 5, 3177-3186(2015).
17. Y. Matsuo, S. Higashika, K. Kimura, Y. Mayamoto, T. Fukutsuka, Y. Sugie, *J. Mater. Chem.* 12, 1592-1596(2002); V. Patil, R. V. Dennis, G. D. Yadav et. al., *RSC Advances*, 4, 49264-49272(2015).
18. S. Stankovich, R. D. Piner, X. Chen, N. Wu, S. T. Nguyen, R. S. Ruoff, *J. Mater. Chem.* 16, 155-158(2006); X. Pu, H. B. Zhang, X. F. Li et. al., *RSC Advances*, 4, 15297-15303(2014).
19. W. H. Liao, S. Y. Yang, C. C. M. Ma et. al. *ACS Appl. Mater. Interfaces*, 5(3), 869-877 (2013); M. Fang, H. B. Lu, Y. L. Yang et. al. *J. Mater. Chem.* 20, 9635-9643 (2010); S. Park, D. S. Kim *Poly. Eng. Sci.* 54, 985-991 (2014).
20. P. Sudhakara, P. Kannan, K. Obireddy, *J. Mater. Sci.*, 46, 2778-2788 (2011).
21. C. A. May, *Epoxy resin: Chemistry and technology. 2th ed*, Marcel Dekker, New York, 1988, pp. 4-10.
22. F. D. Liu, K. K. Guo, *Polymers Advanced technologies*, 25, 418-423 (2014).
23. F. D. Liu, K. K. Guo, J. M. Jian, *High Performance polymers*, 26, 326-334 (2014).
24. Y. X. Xu, H. Bai, G. W. Lu, C. Li, G. Q. Shi, *J Am Chem Soc.* 2008; 130, 5856.
25. C. Nethravathi, M. Rajamathi, *Carbon.* 2008; 46, 1994-1998.
26. M. Rubinstein, R. H. Colby, *Polymer Physics*, Oxford University Press, USA, 2003.
27. S. Stankovich, R. D. Piner, S. B. T. Nguyen, R. S. Ruoff, *Carbon.* 2006; 44, 3342-3347.
28. A. C. Ferrari, J. C. Meyer, V. Scardaci, *Phys. Rev. Lett.*, 97, 187401 (2006).
29. L. Z. Guan, G. Q. Lai et. al., *J. Mater. Chem. A* 2(36), 15058-15069 (2014).
30. M. A. Rafiee, J. Rafiee, I. Srivastava, Z. Wang, H. H. Song, Z. Z. Yu, N. Koratkar, *Small* 6, 179-183(2010).
31. J. C. Meyer, A. K. Geim, M. I. Katsnelson, K. S. Novoselov, T. J. Booth, S. Roth, *Nature.* 446, 60-63(2007).
32. Y. Q. Guo, C. L. Bao, L. Song, B. H. Yuan, Y. Hu, *Ind Eng Chem Res.* 50, 7772-7783(2011).
33. M. L. Sham, J. K. Kim *J. Appl. Polym. Sci* 96, 175-182(2005).

Scheme 1. Synthetic scheme of amine-functionalized graphene oxide nanosheets.

Scheme 2 The mechanism of possible epoxy/amine reactions.

Figure 1 Figure 1 TEM images of GOs (a), D400-GOs(b), and D2000-GOs (c).

Figure 2 (color online) X-ray diffraction (XRD) patterns (a), Thermogravimetric (TGA) curves (b), Fourier transform infrared spectra (c) and Raman spectrum (d) of graphite, graphite oxides(GOs), D400-GOs and D2000-GOs.

Figure 3 (color online)X-ray photoelectron spectroscopy (XPS) of graphene oxides (GOs), D400-GOs and D2000-GOs. (a) Wide scan survey spectra. (b) XPS C1s spectrum of GOs. (c) XPS C1s of D400-GOs. (d) XPS C1s of D2000-GOs. (e) XPS N1s of D400-GOs. (f) XPS N1s of D2000-GOs.

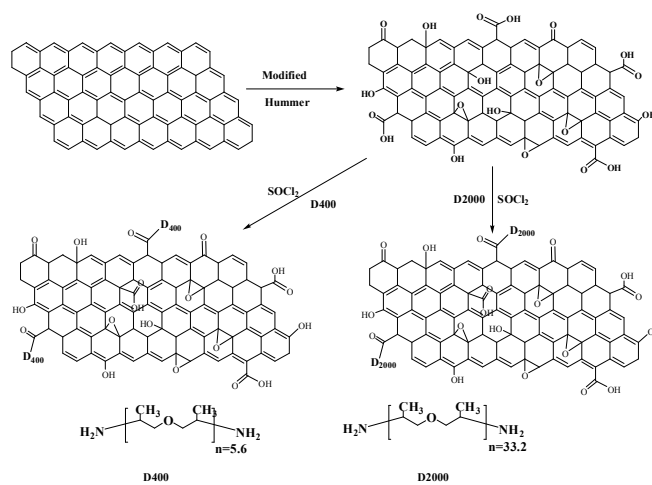
Figure 4 (color online)Tensile properties of D400-GOs/EPs ((a1)-(a3)) and D2000-GOs/EPs ((b1)-(b3)) nanocomposites. (a1) and (b1) Stress-strain curves, (a2) and (b2) Tensile stress, (a3) and (b3) Toughness.

Figure 5 SEM images of the tensile fracture surfaces of the (a1) and (a2) pure EPs, (b1) 0.1 wt.% D400-GOs/EPs nanocomposite, (b2) 0.2 wt.% D400-GOs/EPs nanocomposite, (c1) 0.1 wt.% D2000-GOs/EPs nanocomposite, (c2) 0.2 wt.% D2000-GOs/EPs nanocomposite. Magnification 1000 $\times$ .

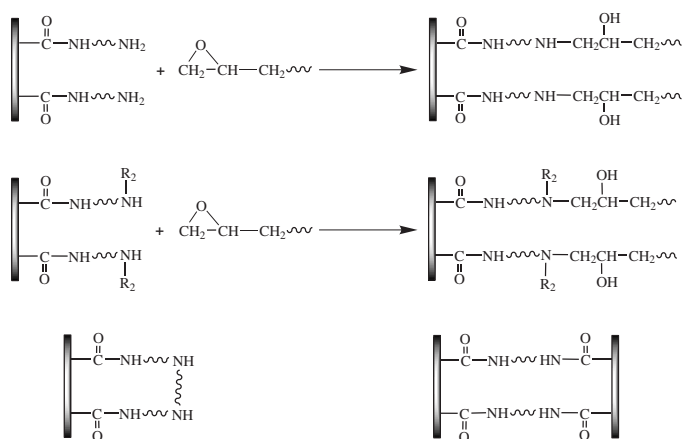
Figure 6 SEM images of the tensile fracture surfaces of (a) 0.2 wt.% D400-GOs/EPs nanocomposite, (b) 0.2 wt.% D2000-GOs/EPs nanocomposite. Magnification 5000 $\times$ . The voids are marked in the circle. ■

Figure 7 (color online) (a) Differential scanning calorimetry curves for the nanocomposites with different loading of D400-GOs and D2000-GOs. (b) Thermogravimetric curves for the nanocomposites with different contents of D400-GOs and D2000-GOs.

Table 1 Thermal property of pure EPs, D400-GOs/EPs and D2000-GOs/EPs composites.



Scheme 1. Synthetic scheme of amine-functionalized graphene oxide nanosheets.



Scheme 2 The mechanism of possible epoxy/amine reactions.

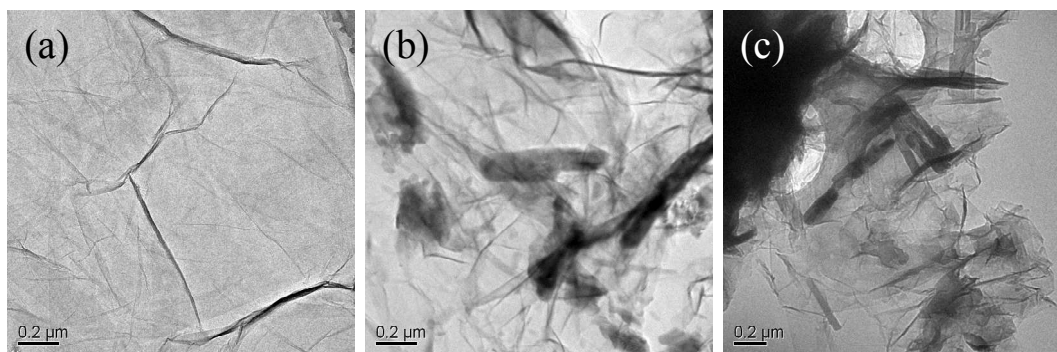


Figure 1 TEM images of GOs (a), D400-GOs(b), and D2000-GOs (c).

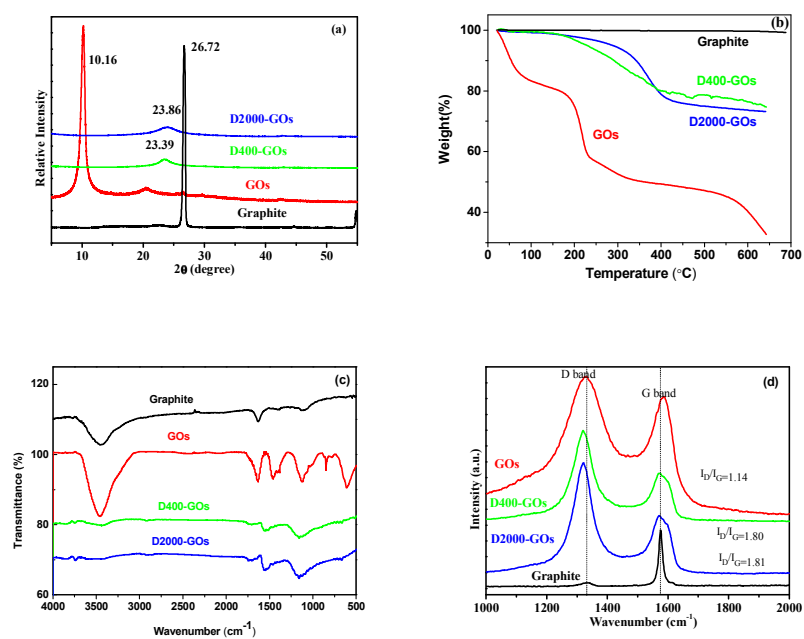


Figure 2 (color online) X-ray diffraction (XRD) patterns (a), Thermogravimetric (TGA) curves (b), Fourier transform infrared spectra (c) and Raman spectrum (d) of graphite, graphite oxides(GOs), D400-GOs and D2000-GOs.

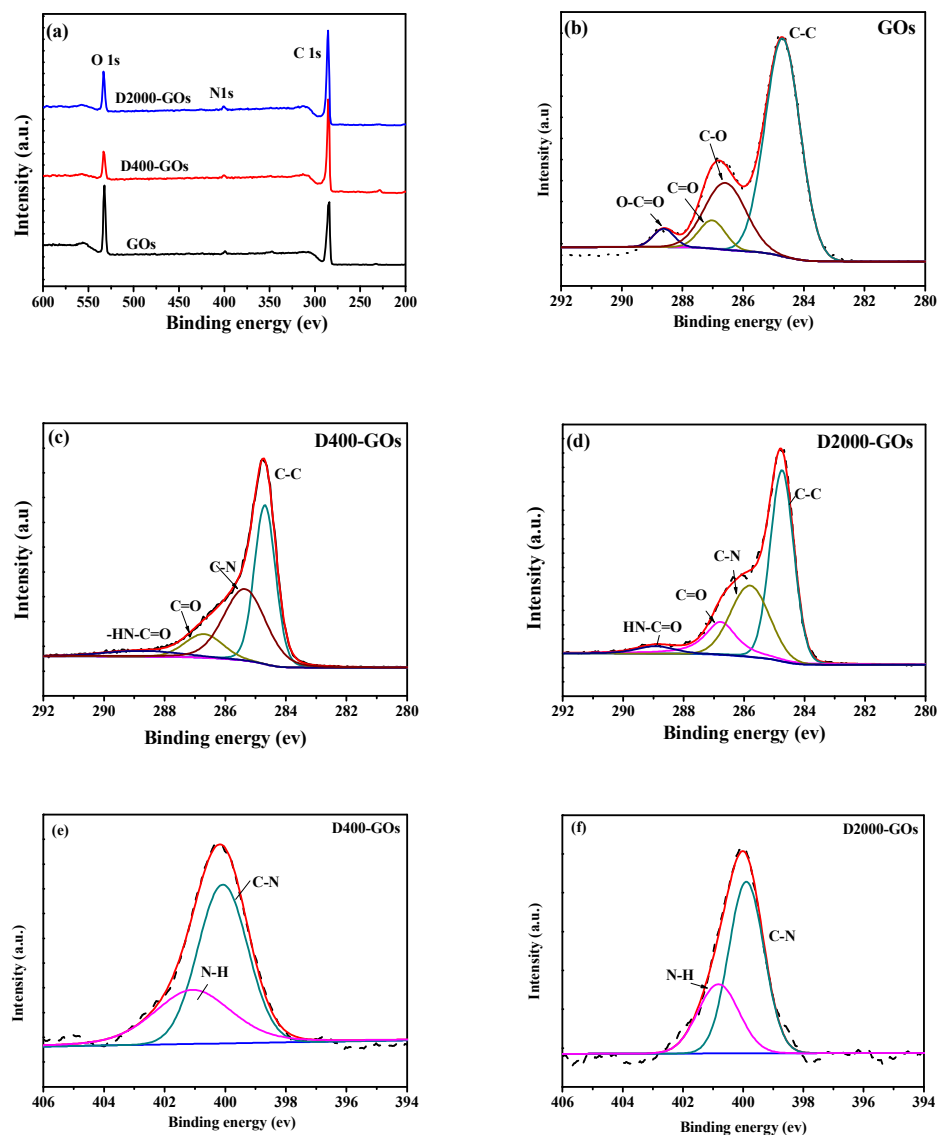


Figure 3 (color online) X-ray photoelectron spectroscopy (XPS) of graphene oxides (GOs), D400-GOs and D2000-GOs. (a) Wide scan survey spectra. (b) XPS C1s spectrum of GOs. (c) XPS C1s of D400-GOs. (d) XPS C1s of D2000-GOs. (e) XPS N1s of D400-GOs. (f) XPS N1s of D2000-GOs.

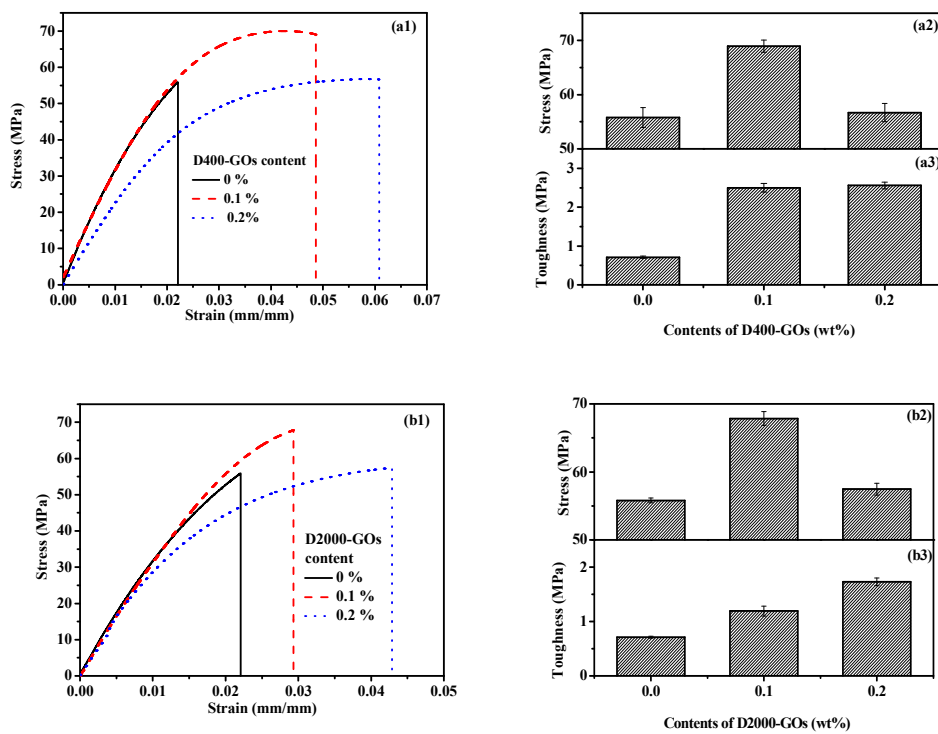


Figure 4 (color online) Tensile properties of D400-GOs/EPs ((a1)-(a3)) and D2000-GOs/EPs ((b1)-(b3)) nanocomposites. (a1) and (b1) Stress-strain curves, (a2) and (b2) Tensile stress, (a3) and (b3) Toughness.

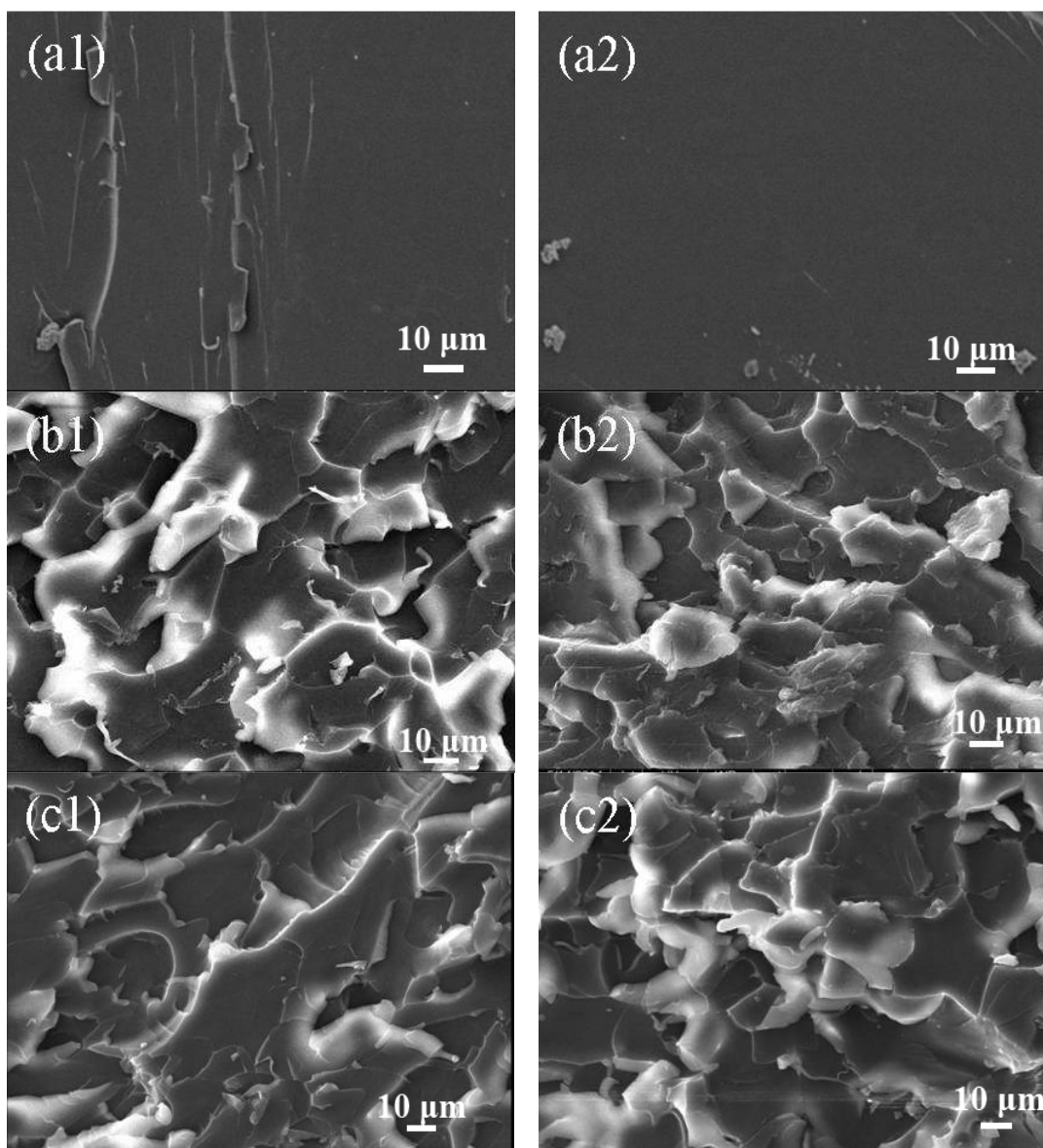


Figure 5 SEM images of the tensile fracture surfaces of the (a1) and (a2) pure EPs, (b1) 0.1 wt.% D400-GOs/EPs nanocomposite, (b2) 0.2 wt.% D400-GOs/EPs nanocomposite, (c1) 0.1 wt.% D2000-GOs/EPs nanocomposite, (c2) 0.2 wt.% D2000-GOs/EPs nanocomposite. Magnification 1000 $\times$ .

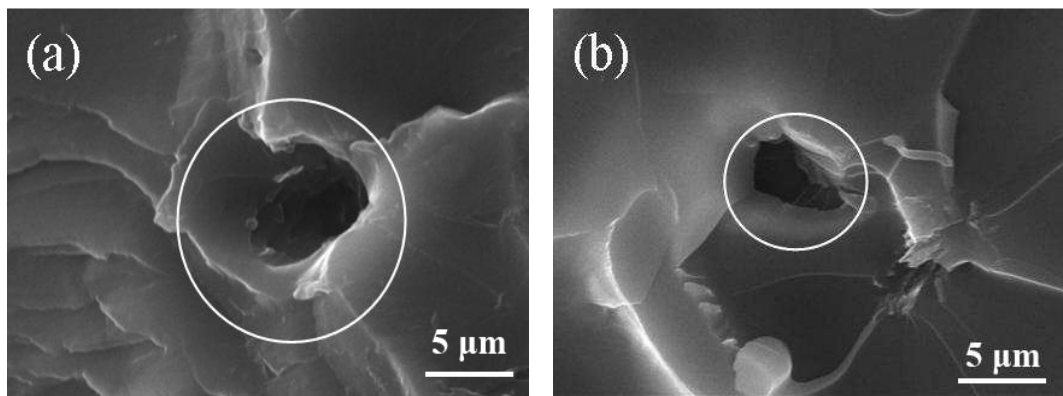


Figure 6 SEM images of the tensile fracture surfaces of (a) 0.2 wt.% D400-GOs/EPs nanocomposite, (b) 0.2 wt.% D2000-GOs/EPs nanocomposite. Magnification 5000 $\times$ . The voids are marked in the circle. ■

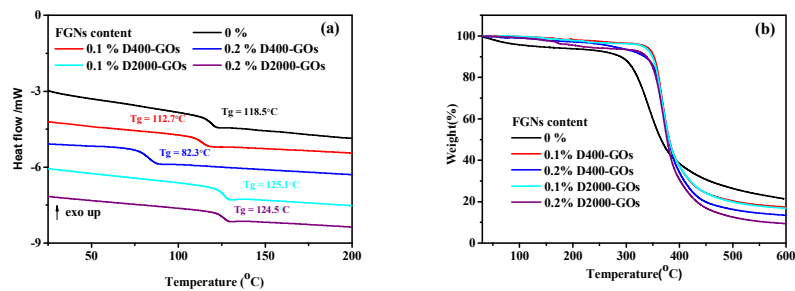


Figure 7. (color online) (a) Differential scanning calorimetry curves for the nanocomposites with different loading of D400-GOs and D2000-GOs. (b) Thermogravimetric curves for the nanocomposites with different contents of D400-GOs and D2000-GOs.

Table 1 Thermal property of pure EPs, D400-GOs/EPs and D2000-GOs/EPs composites.

Materials	T <sub>g</sub> (°C)	T <sub>5%</sub> (°C)	T <sub>50%</sub> (°C)
EPs	118.5	129.6	365.6
0.1 % D400-GOs/EPs	112.7	336.0	381.0
0.2 % D400-GOs/EPs	82.3	263.7	380.0
0.1 % D2000-GOs/EPs	125.1	331.6	380.7
0.2 % D2000-GOs/EPs	124.5	216.6	376.6